



Computational Study of the DNA-Binding Protein *Helicobacter pylori* NikR: The Role of Ni²⁺

Francesco Musiani,^{†,∇} Branimir Bertoša,^{‡,§,∇} Alessandra Magistrato,[‡]
Barbara Zambelli,[†] Paola Turano,^{⊥,‡} Valeria Losasso,[‡] Cristian Micheletti,[‡]
Stefano Ciurli,^{*,†,⊥} and Paolo Carloni^{‡,||}

Laboratory of Bioinorganic Chemistry, University of Bologna, Viale G. Fanin 40,
40127 Bologna, Italy, International School for Advanced Studies (SISSA) and
CNR-IOM-DEMOCRITOS National Simulation Center, via Bonomea 265,
34136 Trieste, Italy, Ruder Bošković Institute, Bijenička 54, 10000 Zagreb, Croatia, German
Research School for Simulation Science, FZ-Jülich and RWTH, Wilhelm-Johnen-Strasse,
52428 Jülich, Germany, Center for Magnetic Resonance (CERM), University of Florence, Via
Luigi Sacconi 6, 50019 Sesto Fiorentino, Italy, and Department of Chemistry, University of
Florence, Via della Lastruccia 3, 50019 Sesto Fiorentino, Italy

Received November 30, 2009

Abstract: An integrated approach, combining atomistic molecular dynamics simulations, coarse-grained models, and solution NMR, was used to characterize the internal dynamics of *Hp*NikR, a Ni-dependent transcription factor. Specifically, these methods were used to ascertain how the presence of bound Ni²⁺ ions affects the stability of the known open, cis, and trans forms observed in the crystal structures of this protein as well as their interconversion capability. The consensus picture emerging from all the collected data hints at the interconversion of NikR among the three types of conformations, regardless of the content of bound Ni²⁺. On the basis of atomistic and coarse-grained simulations, we deduce that the interconversion capability is particularly effective between the cis and the open forms and appreciably less so between the trans conformer and the other two forms. The presence of the bound Ni²⁺ ions does, however, affect significantly the degree of the correlations on the two DNA-binding domains of NikR, which is significantly suppressed as compared to the apo form. Overall, the findings suggest that the binding of *Hp*NikR to DNA occurs through a sophisticated multistep process involving both a conformational selection and an induced fit.

Introduction

Nickel is an essential cofactor for a number of microorganisms.^{1,2} The toxicity of Ni²⁺ imposes control on its homeo-

stasis and cellular trafficking through the regulation of genes expressing proteins involved in nickel metabolism.³ Several human bacterial pathogens rely upon the expression of nickel-dependent enzymes such as urease and hydrogenase to survive in the host organisms,¹ suggesting that a comprehension of the molecular determinants of the regulations of these genes might help in developing efficient drugs. In this biological framework, a key regulator is NikR, a highly homologous protein found across ca. 30 species of bacteria and archaea. Several crystal structures of NikR have consistently established that this protein is a homotetramer made of a dimer of dimers, constituted by a central metal-binding domain (MBD) and two peripheral DNA-binding domains (DBD) (Figure 1, Table 1SI, Supporting Information).^{4–8}

* Corresponding author phone: (+39)-051-2096204; fax: (+39)-051-2096203; e-mail: stefano.ciurli@unibo.it.

[†] University of Bologna.

[‡] International School for Advanced Studies (SISSA) and CNR-IOM-DEMOCRITOS National Simulation Center.

[§] Ruder Bošković Institute.

^{||} German Research School for Simulation Science.

[⊥] Center for Magnetic Resonance (CERM), University of Florence.

[#] Department of Chemistry, University of Florence.

[∇] Francesco Musiani and Branimir Bertoša contributed equally to the simulations presented here.

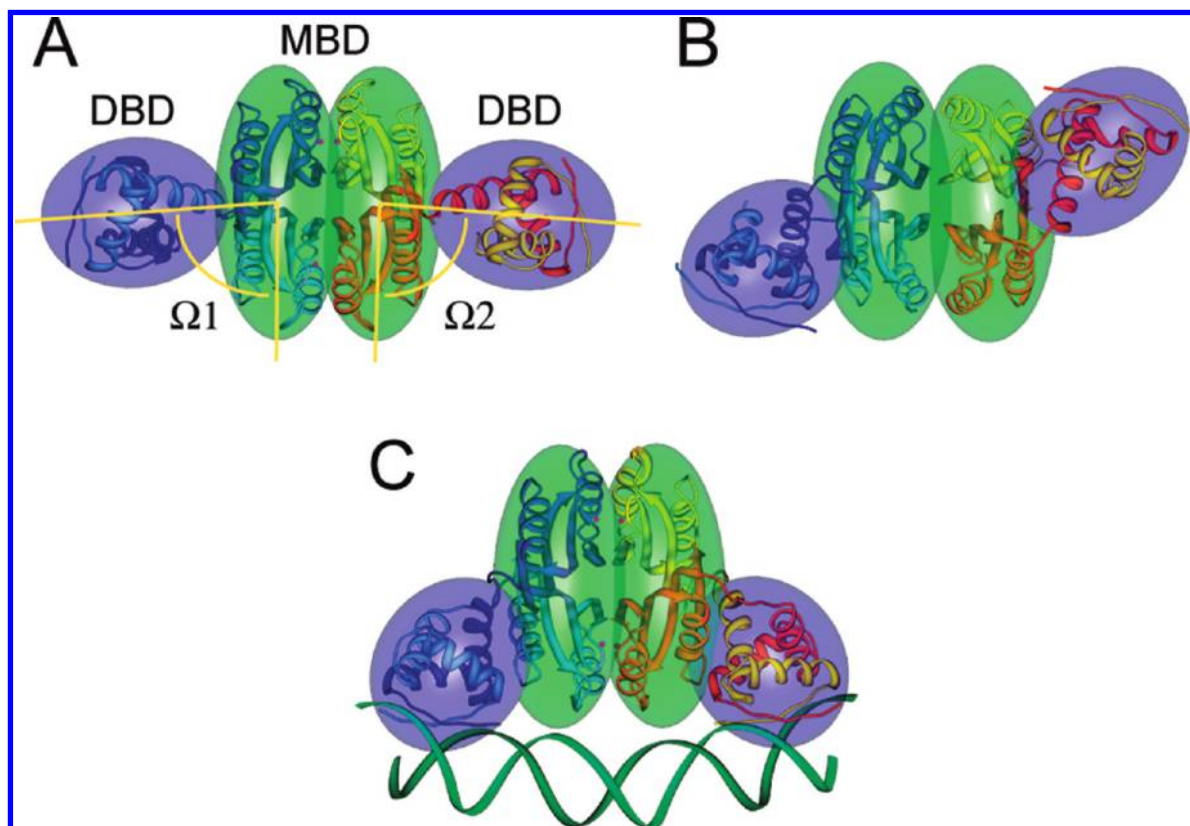


Figure 1. Ribbon diagrams and inertia ellipsoids of NikR in (A) open, (B) trans, and (C) cis conformation (PDB codes 2HZA, 2HZV, 2CA9). In C, the DNA fragment is bound to the protein. Ribbons are colored according to monomer chains. Ellipsoids for DBD and MBD are colored in blue and green, respectively.

The DBD features a ribbon–helix–helix motif typical of prokaryotic transcription factors.⁹ The MBD hosts four metal-binding sites located at the tetramerization interface, where square planar Ni^{2+} ions bind three fully conserved His and one Cys residues.

Three major conformations of NikR, open, trans, and cis, have been observed in the solid-state structures (Figure 1, Table 1SI, Supporting Information). Such conformations are characterized by the position of the peripheral DBDs with respect to the central MBD, separated by unstructured linkers, and are here defined in terms of the two Ω angles between the principal axes of inertial ellipsoids approximating such domains: as a result from the crystal structures, in the open conformation (Figure 1A) Ω_1 and Ω_2 are in the $90 \pm 20^\circ$ range, for the trans conformation (Figure 1B) $\Omega_1 = 45 \pm 20^\circ$ and $\Omega_2 = 135 \pm 20^\circ$, and for the cis conformation (Figure 1C) Ω_1 and $\Omega_2 = 35 \pm 1^\circ$.

Several key studies have identified which protein form binds to DNA in vitro. First, the crystal structure of the *Escherichia coli* (Ec) NikR–DNA complex has shown that the protein must be in its cis conformation (Figure 1C) to interact with DNA.⁶ This conformation, indeed, is complementary to that of the double-stranded nucleic acid and allows for optimal interactions between the peripheral DBDs and DNA.⁶ Second, electrophoretic mobility shift assays, fluorescence anisotropy, DNaseI footprinting, and calorimetric DNA titrations established that only the Ni^{2+} -bound form of NikR specifically binds target DNA sequences, thus providing a direct Ni^{2+} -dependent metabolic response.^{10–13} Third, calorimetric metal-binding titrations on NikR from

the human pathogen *Helicobacter pylori* (HpNikR) revealed two steps for Ni^{2+} binding, each involving a pair of metal ions.¹⁴ This indicates the existence of three metal-bound forms of the protein characterized by the presence of 0, 2, or 4 Ni^{2+} ions. The 4Ni–HpNikR form binds to DNA, while apo–HpNikR does not.¹³ The DNA-binding capability of HpNikR bound to 2 Ni^{2+} ions has so far not been determined due to the too small difference (ca. 1 order of magnitude) in the dissociation constants for the two steps of Ni^{2+} binding.

Overall, these observations indicate that the Ni-bound form of HpNikR binds to DNA in the cis conformation. The key question is therefore what is the role of Ni^{2+} content for modulating the protein affinity for DNA by favoring its reactive cis conformation? This question is far from being answered. The cis conformation has been characterized in the solid state only with 4 bound Ni^{2+} ions in the complex with DNA (Table 1SI, Supporting Information). This contrasts with the open and trans conformations, for which crystal structures without and with 2 or 4 bound Ni^{2+} ions are available (Table 1SI, Supporting Information). It should also be noted that the insights offered from X-ray structures are expectedly limited by crystal packing energetics affecting the conformational properties of DNA-binding proteins like NikR, as suggested by molecular dynamics (MD) simulations.¹⁵

In the absence of solution structural information on the role of Ni^{2+} in the reactivity of NikR toward DNA, insights have been obtained, in recent years, by molecular simulations. A coarse-grained elastic-network model applied to the apo-open, 4Ni-open, and 4Ni-trans conformations of Pyro-

coccus horikoshii (*Ph*) NikR (PDB codes 2BJ3, 2BJ1, and 2BJ7, respectively) suggested the presence of intrinsic fluctuations that are encoded in the protein architecture capable of favoring the interconversion among the conformations observed in the solid-state structures of NikR.¹⁶ Subsequently, the same group reported 100 ns implicit solvent MD simulations on the same systems, concluding that the secondary structure segments involved in binding DNA and Ni^{2+} tend to influence motion across domains much more strongly than other residues and that portions with high flexibility are correlated with biologically relevant regions.¹⁷ In another instance, atomistic 80 ns MD simulations in explicit solvent were analyzed using a correlation-matrix-based approach and hinted to the presence of an allosteric communication pathway between residues in the nickel-binding sites and the DNA-binding region.¹⁸ However, the metal-bound state was not investigated, preventing a comparative study. It should also be noted that this latter atomistic simulation was started from a conformation of the apo form of *Ec*NikR that is somewhat atypical in that the Ω angles observed only in a single-crystal structure (PDB code 1Q5V, Table 1SI, Supporting Information) are between the open and trans conformations. A recent paper describing shorter (ca. 3 ns) MD and Poisson–Boltzmann electrostatic calculations on 4Ni-*Ec*NikR in the open and cis conformations (PDB codes 2HZA and 2HZV) appeared to indicate that the protein–DNA complex is stabilized when 4 Ni^{2+} ions are bound to the MBD.¹⁹

In order to contribute to the understanding of the role of Ni^{2+} on the reactivity of NikR toward DNA binding, we carried out a comparative analysis of atomistic MD simulations (overall 540 ns) of three structure-based homology models of the protein from *H. pylori* in the open, trans, and cis conformations in explicit aqueous solution at finite ionic strength as a function of the absence or presence of 2 or 4 Ni^{2+} ions. The MD simulations were complemented by a state-of-the-art coarse-grained analysis and modeling of the molecule internal dynamics. ^1H – ^{15}N TROSY-HSQC and ^{13}C – ^{13}C NOESY NMR experiments on apo- and 4Ni-*Hp*NikR were also carried out in order to investigate experimentally the structural properties of *Hp*NikR in solution and to link them to the theoretical analysis.

The overall results of this multifaceted approach indicate that NikR is present in solution as an ensemble of interconverting structures spanning the entire conformational space from cis to open to trans forms. The interconversion capability appears to depend on the content of bound Ni^{2+} ions, which in turn affects the motion of the DBDs. The conformational fluctuations are, in addition, finely tuned by the Ni^{2+} content. The NMR solution studies indicate that Ni^{2+} ion binding does not induce, by itself, the stabilization of the cis conformation competent for DNA binding. Overall, these results support the view that the likely mechanism of interaction of the protein with its operator DNA sequence

involves a selection of the correct conformation coupled with an induced fit mechanism facilitated by the presence of bound Ni^{2+} .

Materials and Methods

Structural Models. Initial structural models of *Hp*NikR were obtained using homology modeling based on the available X-ray structures of NikR. The alignment of *Hp*NikR with *Ph*NikR and *Ec*NikR was produced using ClustalW²⁰ and subsequently manually adjusted in order to match up the primary and secondary structure of the proteins. The calculated sequence identity (similarity) between *Hp*NikR and *Ec*NikR is 29% (55%), between *Hp*NikR and *Ph*NikR is 34% (62%), and between *Ph*NikR and *Ec*NikR is 33% (63%). The final alignment (Figure 1SI, Supporting Information) was used to calculate 50 structural models of the open, trans, or cis conformations of tetrameric *Hp*NikR using the program MODELER 9v5.²¹ The structural templates used in each of the conformations were (i) the NikR structures from *P. horikoshii* (PDB code 1BJ1, resolution 3.00 Å) and *E. coli* (PDB code 2HZA, resolution 2.10 Å) for the open conformation, (ii) the DNA-bound *Ec*NikR structure (PDB code 2HZV, resolution 3.00 Å) for the cis conformation, and (iii) the structures of *Hp*NikR (PDB codes 2CA9 and 2CAD, resolution 2.05 and 2.30 Å, respectively) and *Ph*NikR (PDB 2BJ8, resolution 2.10 Å) for the trans conformation.

The models were selected on the basis of the lowest value of the DOPE score in MODELER.²² The structural identity of monomers pairs, depending on the conformation, was imposed. The stereochemical quality of the structures was evaluated using PROCHECK,²³ and the distribution of residual energy was evaluated in ProSA.²⁴ The results of this analysis, reported in Table 2SI, Supporting Information, indicate that the models are highly reliable. Polar hydrogen atoms were added using WHATIF²⁵ by optimizing the hydrogen-bonding networks. During this procedure, few amino acid side chains were allowed to change their orientation. Nonpolar hydrogen atoms were added with TLEAP (AMBER 10).²⁶ Four square planar Ni^{2+} ions were initially included in the model, bound in the known metal binding sites. These metal ions were partially or totally removed from the model depending on whether the apo form, the 2Ni-*Hp*NikR, or the 4Ni-*Hp*NikR was considered. In the case of the 2Ni-bound form, the selection of the two loaded binding sites was made according to the crystal structure of the partially metal-bound form of *Hp*NikR (PDB code 2CAD) independent of the conformation considered. The two nickel ions are located on subunits, giving rise to distinct DBDs, and in opposite positions within the tetrameric cluster.

The models were placed in the center of a water box (113–124, 77–84, and 75–80 Å) using a 10 Å buffer zone of solvent around the protein. The systems were neutralized by adding Na^+ and Cl^- ions using TLEAP (AMBER10).²⁶ The counterions were placed at the points of lowest or highest electrostatic potential, according to a Coulombic potential calculated on a 1.0 Å grid. Analogously, additional Na^+ and Cl^- ions were placed in the water box to achieve the ionic

strength used in the calorimetric binding experiments (150 mM).¹⁴ The number of additional salt ions (61–68 Na⁺ and Cl[−] ions) was calculated according to the number and density of the solvent molecules in each water box. The possible formation of NaCl aggregates during the simulation²⁷ was excluded by calculation of the radial distributions of the ions using the PTRAJ module of AMBER 10.²⁶ The resulting systems consisted of ca. 70 000 atoms.

Force Field. The force field charges for the metal binding sites were obtained by applying DFT calculations on a model consisting of a Ni²⁺ ion coordinated by a methyl-thiolate and three imidazole rings, mimicking cysteine and histidine side chains, respectively. The initial coordinates for this model were taken from the *Ec*NikR structure in the cis conformation bound to its operator DNA (PDB code 2HZV).⁶ The geometry of the initial model was optimized at the B3LYP/6-31G(d) level using tight convergence criteria in the GAUSSIAN software.²⁸ The optimized structure of this model was subjected to single-point calculations in order to derive ESP charges according to the Merz–Kollman scheme.²⁹ RESP charges were obtained with the RESP module of the AMBER 10 software package.²⁶ Force field values for distances, angles, dihedral angles, and partial charges were obtained from the optimized structure (Tables 3–5SI, Supporting Information). Appropriate force field constants were found in the literature.^{30,31} The Amber ff99SB³² and TIP3P³³ force fields were used for the protein frame and water, respectively, while known parameters were used for Na⁺³⁴ and Cl[−].³⁵

Molecular Dynamics. The time step was 1 fs, and the structures were sampled every picosecond. Periodic boundary conditions (PBC) were applied. Particle mesh Ewald (PME) was used to calculate electrostatic interactions. The cutoff values for the real part of the electrostatic interactions and for the van der Waals interactions were set to 10 Å.

Each system was geometry optimized in five cycles of 5000 steps of conjugate gradient. In the first cycle, water molecules were relaxed while the protein was constrained using a harmonic potential with a force constant of 50 kcal mol^{−1} Å^{−2}. In the second cycle, the same constraint was applied to all non-hydrogen atoms. In the third and fourth cycle, only the position of the Ni²⁺ coordination polyhedron was constrained using a harmonic potential with a force constant of 50 and 25 kcal mol^{−1} Å^{−2}, respectively. Finally, in the fifth cycle no constraints were applied.

The systems were subjected to 40 or 100 ns of molecular dynamics (MD) simulations. During the first 240 ps, the temperature was raised from 0 to 300 K at a regular rate of 1.25 K ps^{−1} and keeping the pressure constant (1 atm) using a Berendsen barostat.³⁶ During this time, positional constraints were applied on the protein atoms and Ni²⁺ ions (force constant of 32 kcal mol^{−1} Å^{−2}). Subsequently, 160 ps of MD simulation was run at 300 K using a Berendsen thermostat³⁶ using the same positional constraints. Then, 200 ps of MD simulation was run at 300 K applying the same harmonic potential as above to the protein backbone and Ni²⁺ ions. Finally, in the following 200 ps of MD simulation, only the Ni²⁺ ions were constrained, using the same harmonic

potential. In the subsequent simulations, no constraints were applied and the Berendsen thermostat was used.³⁶

These calculations were performed using NAMD 2.7b1³⁷ running on the IBM Blue Gene/P JUGENE supercomputer (Jülich Supercomputing Centre, JSC, Jülich, Germany) for a total of more than 1 300 000 h of calculation.

Calculated Properties. The Cα root-mean-square deviation (rmsd) was calculated using the minimized structure as reference. On the basis of rmsd vs time plots (see Results section), we calculated averaged properties for the cis and trans conformations after the first 15 ns of simulation. The average number of hydrogen bonds was calculated using the Chimera program³⁸ with its standard parameters. Representative conformations during the dynamics were identified by the clustering analysis of the PTRAJ module of AMBER 10.²⁶ The same module was used to calculate the Na–O, Cl–O, and Na–Cl radial distribution functions, allowing us to exclude formation of NaCl aggregates during the simulation.²⁷ The covariance matrices of pair correlations of the displacements of the Cα atoms were calculated as

$$C_{ij,\mu\nu} = \langle (r_{i,\mu} - \langle r_{i,\mu} \rangle) \cdot (r_{j,\nu} - \langle r_{j,\nu} \rangle) \rangle$$

where $r_{i,\mu}$ is the μ th Cartesian coordinate of the Cα atom of the i th amino acid and $\langle \rangle$ represents the MD average. The calculation was preceded by removal of the rigid-body motions (translations and rotations) accomplished by optimally superposing the MBDs onto the initial reference structure. This procedure, as opposed to aligning the whole molecular complex, removes possible artifactual covariance signals resulting from compensating the displacements of the mobile DBDs with reorientations of the whole NikR molecule. From the covariance matrix we calculated (i) the principal components after matrix diagonalization, (ii) the normalized correlation matrix³⁹

$$C_{ij} = \frac{\sum_{\mu} C_{ij,\mu\mu}}{\sqrt{\sum_{\mu} C_{ii,\mu\mu} \sum_{\nu} C_{jj,\nu\nu}}}$$

(iii) the cREL parameter,¹⁷ which provides an estimate of the relevance of specific residues in inter-residue dynamical relationships

$$\text{cREL}_i = \sum_{\text{chains}} \sum_{j=1}^N |C_{ij}|$$

and (iv) the cFLX parameter,¹⁷ which estimates flexibility as a function of the standard deviation of the distance between consecutive Cα atoms summed over chains

$$\text{cFLX}_i = \sum_{\text{chains}} \sigma(|\overline{x_{i-1}} - \overline{x_{i+1}}|)$$

The protein subdomains were identified by submitting the top 10 principal components to the PiSQRD server (available at <http://pisqrd.escience-lab.org/>).⁴⁰

Coarse-Grained Modeling. The *Hp*NikR internal dynamics were investigated using the β -Gaussian elastic network model,⁴¹ as implemented in an in-house computer program

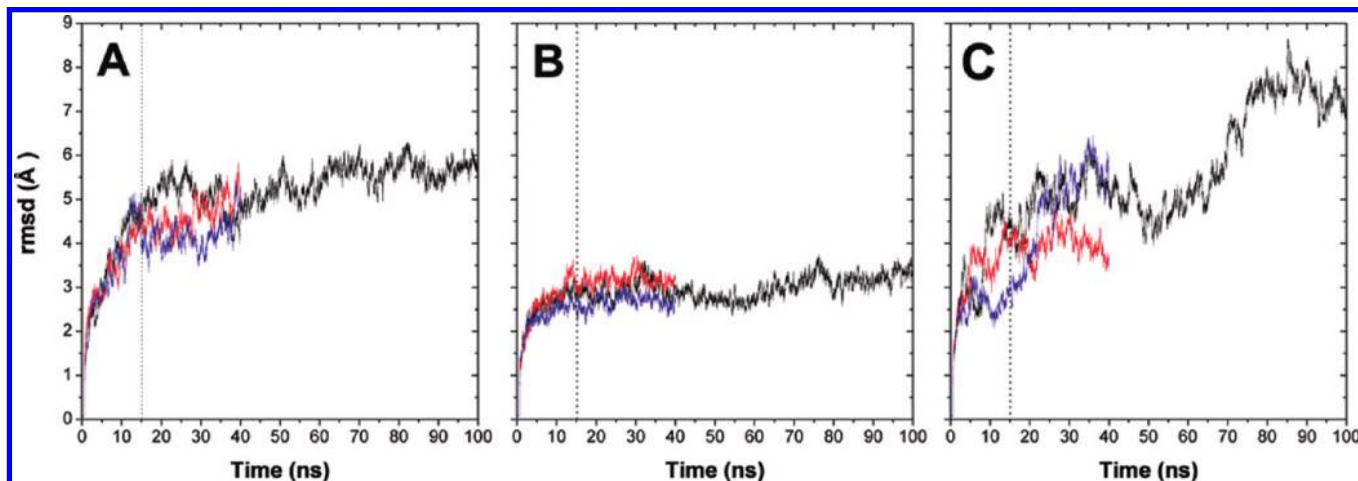


Figure 2. rmsd vs time plots for C α atoms of *HpNikR* in (A) cis, (B) trans, and (C) open conformations. The metalation states of the protein are reported using the black line (apo), red line (2 Ni²⁺ ions), and blue line (4 Ni²⁺ ions). The dotted vertical line in each panel indicates the 15 ns time limit.

freely available for academic use (requests should be directed to C.M.). In the model used, all amino acids are represented by one centroid for the main chain and another for the side chain, except for glycines for which only the former is used. In the case of ENMs based on single-centroid representations, it is necessary to set the range of the harmonic interaction between pairs of interacting centroids to ca. 13–15 Å in order to avoid the appearance of zero-energy modes other than the global translations and rotations of the molecule. The presence of the side chain centroid, while not impacting on the computational complexity of the model, allows us to limit the range of the contact interactions to the more realistic values of ca. 7.5 Å without generating spurious zero-energy modes. In the present context, each bound Ni²⁺ ion was treated as a single effective centroid in the network (as if it were the main chain centroid of a glycine).

NMR Spectroscopy. Triply labeled [98% ²H/¹⁵N/¹³C] apo-*HpNikR* was prepared using *E. coli* BL21(DE3) cells, harboring the pET15b-nikR construct.¹⁴ The cells were grown at 37 °C in Silantes-OD2 medium (Spectra 2000), enriched with 98% of ²H, ¹³C, and ¹⁵N. The expression was induced using IPTG (isopropyl β -thiogalactopyranoside) and carried out at 28 °C for 16 h after induction. Protein purification was carried out as previously reported,¹⁴ yielding 35 mg/L of pure labeled protein. The NMR samples contained 0.5 mM of tetrameric *HpNikR*, diluted in 20 mM HEPES, 150 mM NaCl, at pH 7.0. Solutions of 4Ni-*HpNikR* were prepared by adding a 100 mM solution of NiSO₄ in the same buffer to a final concentration of 2.0 mM.

2D ¹H–¹⁵N TROSY-HSQC experiments⁴² for the apo- and 4Ni-bound protein were carried out at 298 and 315 K on a 21.1-T Bruker AVANCE 900 spectrometer equipped with a TCI cryoprobe. Experiments were acquired with a relaxation delay of 1.2 s and an acquisition time of 87 ms. Typical acquisitions were done with 4 scans for each FID for a matrix of 1024 \times 256 data points.

¹³C–¹³C NOESY maps⁴³ for the apo- and 4Ni-bound protein were acquired on a 16.4 T Bruker AVANCE 700 spectrometer equipped with a triple-resonance observe cryoprobe optimized for ¹³C direct detection at 298 and 315 K. Experiments were acquired with a relaxation delay of 2 s

























and an acquisition time of 29 ms. A mixing time of 1.5 ms was used to allow spin diffusion and detection of side chain complete spin patterns. Composite pulse decoupling on ¹H and ²H was applied during the whole duration of the experiments. ¹³C–¹³C NOESY maps were recorded on the full spectral width (200 ppm) with 64 scans per increment and with 2048 \times 1024 data points.

Results

I. Molecular Dynamics. Hereafter we report on the results of atomistic MD simulations of the three conformers of *HpNikR* in each of the three different metal-bound states, carried out in explicit aqueous solution at 150 mM NaCl ionic strength. The calculations involved a well-established approach^{44–49} that entailed molecular dynamics simulations starting from structures obtained by homology modeling carried out using known structures of NikR from *H. pylori*, *E. coli*, and *P. horikoshii*. This allowed us to prepare a set of consistently built and equally validated structures representing the three conformations present in solutions as sampled by X-ray crystallography. In all cases investigated, both the overall protein fold and the structure of each domain were largely maintained. The rmsds of the cis and trans conformations appear to be converged (Figure 2A and 2B) as opposed to the open conformation, for which convergence is not attained for any of the metal-bound forms (Figure 2C).

Simulation of the *cis*-apo form (Figure 2A) reveals a structural evolution characterized by a considerable widening of one interdomain angle, while the other angle does not change significantly (Table 1). The conformation thus attained peculiarly resembles that of the atypical X-ray structure of apo-*EcNikR* (PDB code 1Q5V). The *cis*-2Ni form tends to evolve toward the open conformation found in the X-ray structures, with a widening of the Ω angles reaching \sim 50°. In the presence of 4 Ni²⁺ ions, the *cis* form evolves toward an asymmetric structure characterized by a ca. 35° increase of one interdomain angle to values typical of the open form (see Table 1SI, Supporting Information) while the other angle decreases by ca. 10°. These data indicate that the *cis* conformer is not dynamically stable independent of the presence of Ni²⁺ ions. In turn, this

Table 1. HpNikR Model Structures and Most Representative Structures During the MD Simulations

Model	Persistence of the most populated cluster (ns)	Average backbone rmsd (Å) (a)	Average Ω_1/Ω_2 angles (°) (b)	Ribbon diagram (c)	Inertia ellipsoid (d)
cis starting model	-	-	34 / 34		
cis - 0 Ni ²⁺	39/85	4.4 (2.1)	41 ± 3 / 78 ± 10		
cis - 2 Ni ²⁺	25/25	3.7 (1.7)	50 ± 4 / 52 ± 3		
cis - 4 Ni ²⁺	18/25	3.7 (1.8)	68 ± 5 / 26 ± 3		
trans starting model	-	-	45 / 135		
trans - 0 Ni ²⁺	55/85	2.9 (1.6)	52 ± 4 / 131 ± 4		
trans - 2 Ni ²⁺	25/25	2.6 (1.5)	45 ± 4 / 143 ± 4		
trans - 4 Ni ²⁺	25/25	2.2 (1.7)	36 ± 5 / 156 ± 5		
open starting model	-	-	88 / 88		
open - 0 Ni ²⁺	10/85	5.5 (2.1)	75 ± 4 / 48 ± 3		
open - 2 Ni ²⁺	7/25	3.5 (1.7)	85 ± 4 / 77 ± 4		
open - 4 Ni ²⁺	10/25	4.5 (3.2)	64 ± 4 / 71 ± 3		

^a rmsd calculated for the most representative cluster of structures. The rmsd calculated superimposing separately the DBD and the MBD domains in order to eliminate the rmsd contribution due to domain movement is reported in parentheses. ^b Ω angles defined as in Figure 1; the average is calculated considering only the most representative cluster of structures \pm one standard deviation. ^c The structure reported is representative of the most populated cluster of structures. ^d The inertia ellipsoids were calculated using the UCSF Chimera software.

suggests that the presence of DNA is necessary to stabilize the correct conformation of NikR for the interaction with its operator.

Simulations of the trans conformation in the presence of 0, 2, or 4 Ni²⁺ ions indicate an overall change in the rmsd (Figure 2B) that is about one-half of that observed for the cis case (~ 3 vs ~ 6 Å) with the Ω angles remaining significantly closer to the initial values independent of the

Ni²⁺ content (Table 1). This observation indicates that this conformer is relatively more resilient to change the inter-domain orientation as compared to the cis form. The large movements observed for the open conformation, overall spanning a range of 4–8 Å (Figure 2C) and leading to the lack of convergence of the rmsd independent of the Ni²⁺ content, suggests that in this case the protein is able to explore a shallower free energy landscape. At present, a much

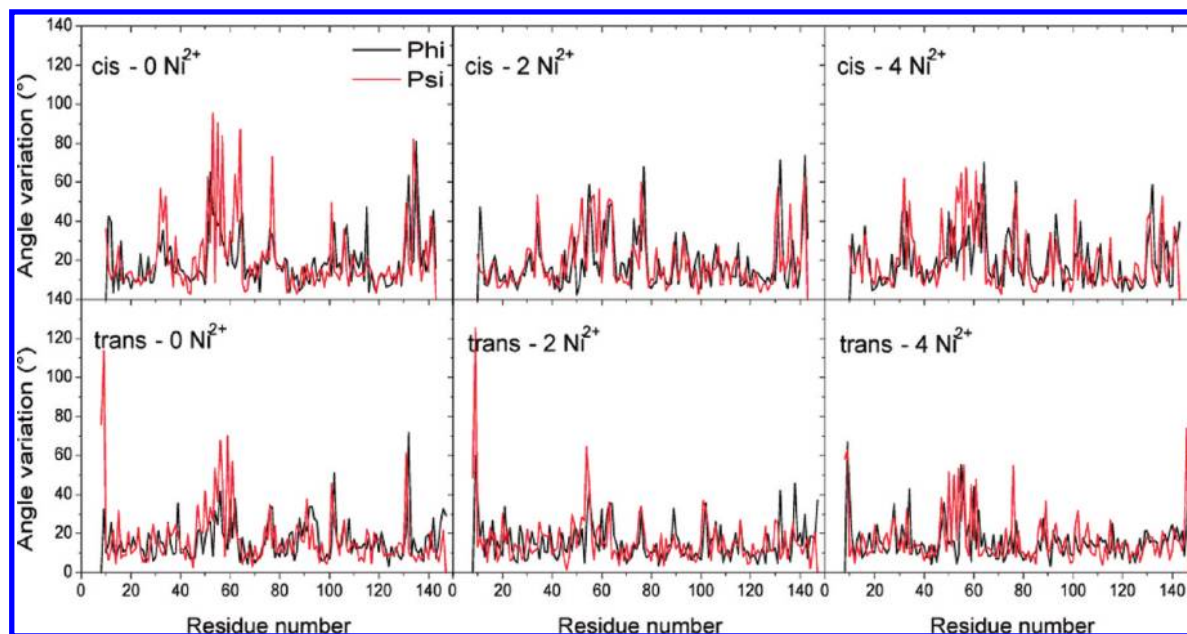


Figure 3. Backbone torsional angle analysis for *HpNikR* in cis (top panels) and trans (bottom panels) conformations in different metalation states: apo (left panels), 2Ni^{2+} ions (central panels), and 4Ni^{2+} ions (right panel). The plots report the absolute value of the difference between the angles in the structure representative of the most populated cluster and those in the minimized starting structure. Φ angles are reported with black lines, while Ψ angles are reported with red lines.

longer time scale simulation of such large systems appears not to be feasible even in the largest supercomputers available, such as the one used for this work. The lack of convergence for the open conformations induced us not to carry out a detailed analysis of the structural parameters for this case.

An analysis of the average number of H bonds in the various metal-bound states of all structures belonging to the most representative cluster revealed that the trans conformation is characterized by ca. 10% more H bonds as compared to the cis conformation, independent of the Ni^{2+} content. This is contrasted by the ca. 15% decrease of the number of H bonds within four shells around the metal-binding sites observed in the case of the trans vs cis conformer. These observations support the view that, in the case of the trans form, the nickel binding relaxes the structure in the MBD while enhancing, on the other hand, the rigidity of the overall protein architecture.

To pinpoint the protein regions involved in the observed structural changes during the MD simulations of the cis and trans conformers, we carried out an analysis of the backbone dihedral angles Φ and Ψ as a function of residue number (Figure 3). Two regions were detected as undergoing variations consistently among all cis and trans conformers: residues 50–60 (the linker between the MBD and the DBD) and residues 30–35 (a loop connecting the first and second helix in the DBD domain). This reveals the presence of two subdomains in the DBDs. No significant differences of the variations of dihedral angles were observed either upon changing the Ni^{2+} content or between the two conformations.

The correlation and flexibility parameters cREL and cFLX can be used to estimate, respectively, the structural stability and instability of proteins regions.¹⁷ Plots of cREL as a function of residue number for the cis and trans conformations (Figure 4A and 4B, respectively) allow us to propose

that the presence of 2 or 4 Ni^{2+} ions causes an increase of disorder of the MBD region in contact with the DBD (residues ca. 110–140). Moreover, addition of Ni^{2+} ions in the trans conformation also increases disorder in the protein region starting from the linker between the MDB and DBD and extending to the metal-binding portion (residues 55–110). Plots of cFLX for the same conformers (Figure 4C and 4D) show the presence of a very flexible region corresponding to the linker between the DBD and the MBD as well as a flexible portion that divides the DBD into two subdomains in correspondence of the loop between the first and the second α -helix, consistent with the analysis of the dihedral angles. Other minor regions of high flexibility correspond to loops between elements of secondary structure throughout the protein.

Motion correlations between various subparts of the protein can be identified by a calculation of the covariance matrices of the amino acids displacements. Visual inspection of the corresponding maps (Figure 5) immediately conveys the remarkable fact that in the cis conformation the motion of the two DBDs is anticorrelated, meaning that they move along opposite directions, with both Ω angles tending to concomitantly increase or decrease. In contrast, in the trans conformation the two DBDs have a positive motion correlation. The results, supported by inspection of the covariance principal components, indicate that the internal fluctuations of the cis conformation favor a scissor-like movement of the DBDs while the trans conformation tends to maintain a collinear geometry of the DBDs. Hence, the internal dynamics of both the cis and the trans forms can facilitate their conversion to the open conformer. For the considered conformations, the simulations with bound Ni^{2+} ions display an appreciable decrease of the absolute magnitude of the DBDs correlation with respect to the simulations of the apo forms. (We recall that the apo simulations have a longer

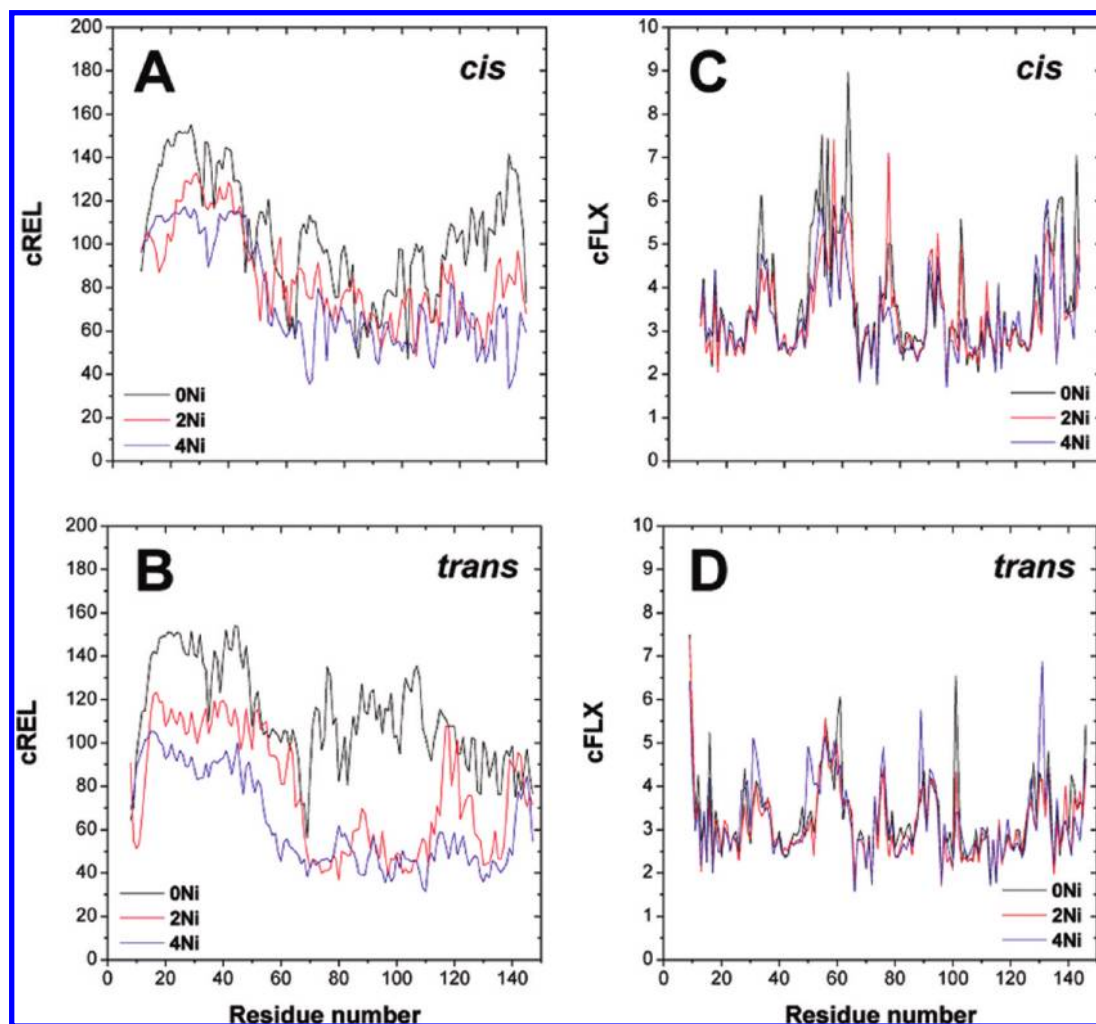


Figure 4. Correlation relevance summed over chains (cREL, A and B) and residue flexibility (cFLX, C and D) for the cis and trans simulations. The metalation states of the protein are reported using black lines (apo), red lines (2 Ni²⁺ ions), and blue lines (4 Ni²⁺ ions).

duration (100 ns) compared to those with the bound metal ions (40 ns), yet the described DBD correlations are maintained independent of the different simulation durations. This was ascertained by verifying the consistency of the correlation matrix shown in Figure 5 with that restricted to the 40 ns simulation time.) These results indicate that the degree of correlation of the DBDs motion depends on the content of Ni²⁺ ions. This fact suggests that the presence of nickel affects the interconversion capability across the various NikR conformers, causing a loss of correlated motion of the DBD domains. Interestingly, for both the trans and the cis trajectories the loss of correlation is not accompanied by an appreciable decrease of the overall mobility of the domains. In fact, the total mean square fluctuation of the molecule, calculated over the 15–40 ns interval, remains approximately equal to 1100 Å² for the cis simulations and about 660 Å² for the trans case irrespective of the number of bound Ni²⁺ ions.

Further insights into the large-scale internal motions of *Hp*NikR can be obtained by a suitable analysis of the most representative conformations for the various trajectories. In particular, the principal components of the covariance matrix computed over the nine MD most representative structures were processed by the PiSQRD online tool⁴⁰ with the aim

of identifying the protein quasi-rigid dynamical subdomains. The number of optimal quasi-rigid domains depends on the amount of overall structural fluctuations of the system (the mean square deviation of the nine MD most representative structures) that one wishes to capture in terms of the relative motion of quasi-rigid subparts.⁵⁰ By considering simultaneously the ensemble of all such conformers visited by all the trajectories it is possible to identify the main dynamical subdomains whose relative, rigid-like motion is sufficient to reproduce the breadth of the heterogeneous conformational space visited by all the trajectories, including the configurational space spanned by the slowly converging open simulations.

Nearly 50% of the mean square deviation (MSD) across the structure representatives of the nine trajectories is ascribable to the relative movements of the two DBDs with respect to the central MDB. The subdivision indicates that the linkers between the MDB and the DBDs act as retractable hinges for the DBD motion. In fact, on the one hand, the two DBDs are capable of rotating around the ideal hinge axis connecting the two linkers and, on the other hand, the separation of the DBD from the MDB depends on the degree of stretching of the linkers themselves. Throughout the various trajectories, the central core maintains its structure, with only minor

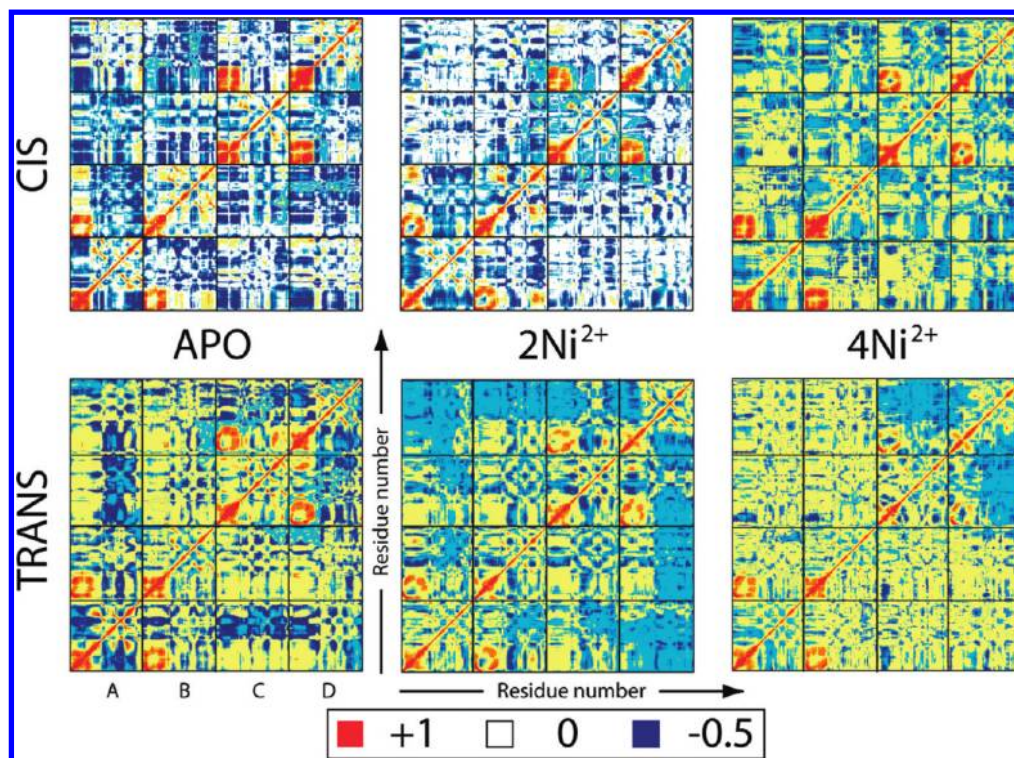


Figure 5. Residue–residue-based map of $C\alpha$ correlation matrices of *HpNikR* in cis (top panels) and trans (bottom panels) conformations. Red and orange regions show positive correlation, while dark blue regions indicate anticorrelation. The black lines indicate the border between one chain and the subsequent chain.

internal deformations. Indeed, upon increasing to five the number of quasi-rigid domains, so to capture an even larger fraction of the ensemble MSD, it is found that the central core is still recognized as a single rigid unit while each of the DBD is split in two subunits. A minor but still sizable fraction of the *HpNikR* conformational variability resides in the internal mobility of each of the two DBD, as signaled by the fact that the subdivision in five units captures ca. 70% of the ensemble MSD. Consistent with the analysis of dihedral angles and the cFLX parameter, the internal dynamical boundary of the DBDs separates the part closest to the MBD from the most peripheral protein portion constituted by amino acids 8–42 on one chain and 8–21 on the other chain.

The results from this coarse-grained perspective indicate that the structural variability of *HpNikR* observed across the nine trajectories is accountable by the relative roto-translational motion of very few quasi-rigid subparts that are connected by motion hinges, fully consistent with the indications of the dihedral angles analysis.

II. Coarse-Grained Modeling. In light of previous studies^{17,18} it appears most interesting to ascertain whether the large-scale internal motions of *HpNikR* are encoded in the overall structural organization of the protein or if they are influenced by fine chemical aspects, such as the presence of bound Ni^{2+} ions. We tackled these questions using the β -Gaussian elastic network model (ENM).⁴¹ Because of its minimalistic character, the model highlights the internal dynamic properties that are robustly encoded in the overall structural organization of a protein. The specific model employed here differs from that previously used for NikR¹⁸ by the fact that the amino acids are represented by more

than one interaction center (or centroid, see Methods for details). This has been shown to improve the consistency of the model predictions (covariance and correlation matrices, essential dynamical spaces) with results from extensive atomistic MD simulations.^{41,51–53}

The model was accordingly used to compute the 10 lowest energy modes of fluctuations of the main structural representatives for each of the six cis and trans trajectories; because of the lack of convergence of the open MD trajectories, the three initial energy-minimized open structures were used. In a similar spirit to previous work,¹⁸ we ascertained whether the low-energy modes can assist the open, cis, and trans interconversions at a fixed number of bound Ni ions by projecting the structure difference vector of various pairs of representatives (aligned over the common set of amino acids) on the space of the 10 lowest energy modes of either representative. We found that irrespective of the number of bound Ni^{2+} ions, the 10 lowest energy modes of the open structures could account for $48 \pm 9\%$ of the difference vectors with either the cis and trans conformations. Comparable results were found for the cis structures, whose modes captured about $43 \pm 9\%$ of the difference vectors with either the open or trans form. The worst compliance of the lowest energy modes with the difference vectors was observed for the trans form. Indeed, only about $36 \pm 12\%$ of the difference vectors with the open or cis form was projected on the lowest energy modes of the trans structure. This result appears to be highly consistent with the analysis of the MD covariance matrices described above, which indicates a facilitated interconversion from the cis to the open form, while the internal dynamics of the trans

conformer is not particularly prone to interconvert toward the two other conformations.

A notable difference between the results obtained using the elastic-network model as compared to the observations derived from the MD analysis is that, in the first case, no significant differences are observed as a function of the number of bound Ni^{2+} . Overall, the results of ENM calculations confirm previous observations^{17,18} that the structural architecture of NikR is predisposed to sustain low-energy fluctuations that can assist the interconversion between different NikR forms. In addition, the MD covariance analysis reveals that the presence of the bound metal ions can significantly alter the internal dynamics and hence impact on the interconversion dynamics.

III. NMR Spectroscopy. To investigate the structural determinants of the protein at longer time scales than those studied by MD, we performed NMR measurements of the protein in solution at the same ionic strength as that of the simulations and at temperatures (298–315 K) that include that of our MD simulations. The ^1H – ^{15}N TROSY-HSQC spectrum of apo *HpNikR*, which provides information on the structural features of the backbone, shows a number of peaks consistent with the number of amino acids in the protein sequence (Figure 6A, black trace). This observation points to the presence, in solution, of the apo form of the protein either in the single open symmetric conformation or undergoing conformational equilibria with submilliseconds interconversion among various conformers. Concomitantly, these results exclude the presence of only the rigid cis or rigid trans conformations in solution, for which two sets of resonances would be expected because of the different structures of the linker regions between the MBD and the DBDs for each monomer. The same situation holds for the ^1H – ^{15}N TROSY-HSQC spectrum of the 4Ni-bound *HpNikR* (Figure 6A, red trace), indicating that the presence of 4 Ni^{2+} ions bound to the protein does not induce a conformational change to a rigid cis form. Over the investigated range of temperatures (298–315 K), signals remain sharp and no signal splitting is observed. While this does not allow us to distinguish between the rigid symmetric or the fluxional behaviors described above using NMR, the presence of the rigid open conformation in solution can be excluded on the basis of our MD and coarse-grained calculations.

^{13}C – ^{13}C NOESY maps of both apo- and 4Ni-bound *HpNikR* provide information on the structural features of the side chains. In these maps, intraresidue cross peaks could be easily detected for most residues due to the spin-diffusion effects operative at the long mixing time used in these experiments (Figure 6B). By taking advantage of the residue-specific chemical shifts of carbon nuclei resonances and using intraresidue NOESY connectivities, we were able to identify the spin patterns of most aliphatic residues and of some aromatic residues. This allowed us to verify that the number of spin patterns observed for a given type of amino acid corresponds to the frequency of that residue type in the protein sequence (this is, for example, the case of isoleucine (a) and alanine (b) residues indicated in Figure 6B). Therefore, no distinct conformations, on the chemical shift

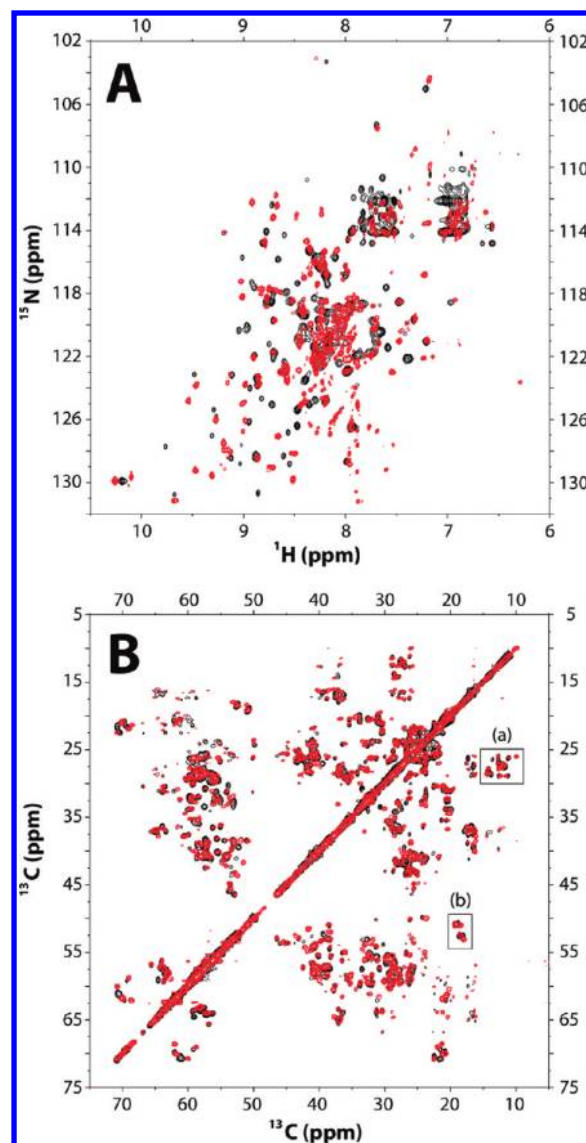


Figure 6. Superimposition of the NMR spectra for [^2H , ^{13}C , ^{15}N] apo-*HpNikR* (black trace) and 4Ni-*HpNikR* (red trace): (A) ^1H – ^{15}N TROSY-HSQC spectra at 315 K; (B) aliphatic region of the ^{13}C – ^{13}C NOESY at 315 K. Insets a and b in the NOESY spectrum correspond to the region of the $\text{C}\gamma_1$ – $\text{C}\delta$ connectivities for Ile residues and to the region of the $\text{C}\alpha$ – $\text{C}\beta$ connectivities for Ala residues, respectively.

NMR time scale, are observed for any side chains of the identified amino acids.

Comparison of the spectra of the apo- and 4Ni-protein shows significant differences in the chemical shift of the backbone amides (in the TROSY-HSQC) and side chain carbon nuclei (in the ^{13}C – ^{13}C NOESY) for the two metalation states. The ^1H – ^{15}N TROSY-HSQC patterns can be taken as a fingerprint for backbone structure of the differently metal-bound protein forms. The existence of a backbone structure signature for each metal-bound state translates into different spectral patterns for the side chains in ^{13}C – ^{13}C NOESY maps. Our NMR data indicate that the presence of Ni^{2+} does affect the position of the conformational equilibria occurring on the submilliseconds time scale. On the other hand, MD simulations do not show Ni-dependent changes in the structural interconversion on the multnanoseconds

time scale. Taken together, the two independent sets of information provide a time range for the equilibria among different structures.

Discussion

Several issues involving the role of Ni^{2+} ions in the structure–function relationships of *H. pylori* NikR, a nickel-dependent transcription regulator, have been addressed in this study using computational and theoretical tools as well as solution NMR experiments. The techniques were combined to gain insight into the capability of *Hp*NikR to interconvert between the main distinct structural states found in crystal structures, namely, the open, cis, and trans states. In particular, the questions that we addressed concern (i) the structure and conformational fluctuations of the protein in a relatively short time scale (tens of nanoseconds) using atomistic MD simulations in explicit solvent, and at longer time scales, using coarse-grained MD analysis and modeling, as well as NMR experiments, (ii) the role of Ni^{2+} in promoting the cis conformation, known to bind DNA, as opposed to the open or trans conformations, (iii) the mechanism by which the active cis conformation interacts with DNA, investigating whether the NikR–DNA interaction occurs through an induced fit mechanism or a conformation selection in solution or a combination of both.

Our MD simulations allow us to suggest that within the time scale of few tens of nanoseconds, the cis conformation in solution evolves toward the open form found in the solid state.⁶ The trans conformation in solution features a significantly higher resilience to change its morphology. A key region of the protein undergoing local changes upon Ni^{2+} binding is the loop acting as a hinge between two subdomains of each DBD.

In particular, the open conformation did not reach convergence in a relatively long time scale for this large system (up to 0.1 μs for the apo form), pointing to a larger degree of structural mobility than that of the other two forms. This hampered any analysis of the structural parameters. However, this finding does suggest that the observation of a specific conformation for this protein form in the solid state (Table 1SI, Supporting Information) might be the result of crystal packing effects, which may not be maintained in solution. Most likely, also the Ni-bound forms do not converge in a similar time scale, although we were able to explore only up to 0.04 μs for these forms. NMR experiments, performed here in the same conditions as those of the MD simulations, indicate that a much longer time scale, up to a millisecond, might be required for the system to reach equilibration. In fact, the symmetric average structure found by NMR combined with the known fact that *Hp*NikR in solution binds DNA in an asymmetric (cis) conformation indicate not only that conformational states with different symmetry exist in solution but that they also interconvert on the submillisecond time scale.

The tendency of Ni^{2+} to increase the motional disorder of flexible protein regions at the interface between the MBD and the DBD was observed in both the cis and trans conformers by MD simulations. In the absence of metal ions, the motion of the DBDs with respect to the MBD is

anticorrelated in the case of the cis conformer: this indicates that the protein architecture is intimately designed to move in a scissor-like mode, producing a concerted modulation of the distance of the DNA-binding regions and therefore favoring an induced fit recognition mechanism. On the other hand, the interdomain movement is positively correlated in the case of the trans conformation. This is consistent with a possible evolution of this conformer initially toward the open and subsequently to the cis form in order to be activated for DNA binding. This view is supported by the analysis based on elastic networks, which indicated that the internal dynamics of *Hp*NikR conformers in the open and cis forms favor their mutual interconversion. On the other hand, the internal dynamics of trans conformers were found less favorable for their interconversion toward the other forms compatibly with the lower DBDs mobility found in MD simulations for these conformers compared to the case of cis conformers.

In the presence of 2 or 4 Ni^{2+} ions these correlated motions decrease, suggesting that the presence of Ni^{2+} ions unlocks the reciprocal orientations of the DBDs vs the MBD. The dependence of the correlation pattern on the number of bound metal ions was systematically observed across all types of conformations and hence points to a robust mechanism through which the Ni^{2+} ions binding in a rigid part of the molecule can influence the dynamics of the peripheral domains.

As mentioned above, our MD calculations suggest that the presence of Ni^{2+} ions affects the conformational fluctuations. However, it does not significantly change the average structures in the time scales investigated by our MD simulations. The high CPU cost of the latter prevented us from further prolonging the simulations. Then, to address this issue, we performed high-resolution NMR spectroscopy on *Hp*NikR in solution at the same ionic strength as in the simulations. These experiments reveal that the presence of Ni^{2+} does affect the structure of the protein but by itself the binding of these ions is not sufficient to attain the sole cis form in solution. Hence, additional effects, such as the presence of DNA causing a blockage of a conformational fluxional behavior of the protein, must operate in solution to yield the NikR–DNA complex.

The overall picture emerging from our study is consistently interpreted within the most recent and general interpretative frameworks for protein–macromolecule interaction.⁵⁴ NMR studies here indicate that NikR is present in solution either in a single symmetric conformation or as an average ensemble of conformers interconverting on the submillisecond time scale. However, it is the asymmetric cis conformer (suggested to be stable in solution by our simulations) that binds selectively to DNA, as shown by X-ray crystallography.⁶ The open conformation, also suggested to be stable in solution by MD calculations, is symmetric and fully consistent with NMR data. Other conformations, such as the crystallographically established trans conformation, found to be stable in aqueous solution by MD simulations, could also be present. Hence, here we speculate that the cis conformation (and maybe other conformations such as the trans) are in equilibrium with the symmetric open conformation in the

submilliseconds time scale or less. The proposed picture is fully consistent with NMR data. It needs to be further validated against calculations and/or experiments.

The conformational change from the open (and perhaps other conformers such as the trans) to the cis form must occur upon DNA binding. The observed effect of the bound Ni^{2+} ions in unlocking the relative movement of the DBDs vs the MBD could be instrumental to facilitate protein–DNA molecular recognition. Of course, it cannot be ruled out that the molecular-recognition step is aided by a concurrent induced fit step. Further investigations of these aspects, by means of computational techniques such as advanced thermodynamic sampling as well as simulations using the structure of the PhNikR, ought to provide further elements to pinpoint the key steps governing the Ni-regulated interaction of NikR and DNA.

Acknowledgment. Computational resources were granted by CINECA (CNR-INFM grant) and by the German Research School. B.B. was a recipient of a grant based on the project “New Antitumoral Technologies”; F.M. was a recipient of a postdoctoral fellowship from UniBO and of a fellowship from CERM-CIRMMP. Work was supported by Italian PRIN2007.

Supporting Information Available: Details of the results of the MD simulations. This material is available free of charge via the Internet at <http://pubs.acs.org>.

References

- Mulrooney, S. B.; Hausinger, R. P. *FEMS Microbiol. Rev.* **2003**, *27*, 239–261.
- Ragsdale, S. W. *J. Biol. Chem.* **2009**, *284*, 18571–18575.
- Li, Y.; Zamble, D. B. *Chem. Rev.* **2009**, *109*, 4617–4643.
- Schreiter, E. R.; Sintchak, M. D.; Guo, Y.; Chivers, P. T.; Sauer, R. T.; Drennan, C. L. *Nat. Struct. Biol.* **2003**, *10*, 794–799.
- Chivers, P. T.; Tahirov, T. H. *J. Mol. Biol.* **2005**, *348*, 597–607.
- Schreiter, E. R.; Wang, S. C.; Zamble, D. B.; Drennan, C. L. *Proc. Natl. Acad. Sci., U.S.A.* **2006**, *103*, 13676–13681.
- Dian, C.; Schauer, K.; Kapp, U.; McSweeney, S. M.; Labigne, A.; Terradot, L. *J. Mol. Biol.* **2006**, *361*, 715–730.
- Phillips, C. M.; Schreiter, E. R.; Guo, Y.; Wang, S. C.; Zamble, D. B.; Drennan, C. L. *Biochemistry* **2008**, *47*, 1938–1946.
- Chivers, P. T.; Sauer, R. T. *Protein Sci.* **1999**, *8*, 2494–2500.
- Chivers, P. T.; Sauer, R. T. *J. Biol. Chem.* **2000**, *275*, 19735–19741.
- Chivers, P. T.; Sauer, R. T. *Chem. Biol.* **2002**, *9*, 1141–1148.
- Dosanjh, N. S.; Michel, S. L. *Curr. Opin. Chem. Biol.* **2006**, *10*, 123–130.
- Zambelli, B.; Danielli, A.; Romagnoli, S.; Neyroz, P.; Ciurli, S.; Scarlato, V. *J. Mol. Biol.* **2008**, *383*, 1129–1143.
- Zambelli, B.; Bellucci, M.; Danielli, A.; Scarlato, V.; Ciurli, S. *Chem. Commun.* **2007**, 3649–3651.
- Berrera, M.; Pantano, S.; Carloni, P. *J. Phys. Chem. B* **2007**, *111*, 1496–1501.
- Cui, G.; Merz, K. M., Jr. *Biophys. J.* **2008**, *94*, 3769–3778.
- Sindhikara, D. J.; Roitberg, A. E.; Merz, K. M. *Biochemistry* **2009**, *48*, 12024–12033.
- Bradley, M. J.; Chivers, P. T.; Baker, N. A. *J. Mol. Biol.* **2008**, *378*, 1155–1173.
- Phillips, C. M.; Nerenberg, P. S.; Drennan, C. L.; Stultz, C. M. *J. Am. Chem. Soc.* **2009**, *131*, 10220–10228.
- Thompson, J. D.; Higgins, D. G.; Gibson, T. J. *Nucleic Acid. Res.* **1994**, *22*, 4673–4680.
- Marti-Renom, M. A.; Stuart, A. C.; Fiser, A.; Sanchez, R.; Melo, F.; Sali, A. *Annu. Rev. Biophys. Biomol. Struct.* **2000**, *29*, 291–325.
- Shen, M.; Sali, A. *Protein Sci.* **2006**, *15*, 2507–2524.
- Laskowski, R. A.; MacArthur, M. W.; Moss, D. S.; Thornton, J. M. *J. Appl. Crystallogr.* **1993**, *26*, 283–291.
- Wiederstein, M.; Sippl, M. J. *Nucleic Acids Res.* **2007**, *35*, W407–W410.
- Vriend, G. *J. Mol. Graph.* **1990**, *8*, 52–56.
- Case, D. A.; Darden, T. A.; Cheatham, T. E., III; Simmerling, C. L.; Wang, J.; Duke, R. E.; Luo, R.; Crowley, M.; Walker, R. C.; Zhang, W.; Merz, K. M.; Wang, B.; Hayik, S.; Roitberg, A.; Seabra, G.; Kolossváry, I.; Wong, K. F.; Paesani, F.; Vanicek, J.; Wu, X.; Brozell, S. R.; Steinbrecher, T.; Gohlke, H.; Yang, L.; Tan, C.; Mongan, J.; Hornak, V.; Cui, G.; Mathews, D. H.; Seetin, M. G.; Sagui, C.; Babin, V.; Kollman, P. A. *AMBER10*; University of California: San Francisco, 2008.
- Auffinger, P.; Cheatham, T., III. *J. Chem. Theory Comput.* **2007**, *3*, 1851–1859.
- Frisch, M. J.; Trucks, G. W.; Schlegel, H. B.; Scuseria, G. E.; Robb, M. A.; Cheeseman, J. R.; Montgomery, J. A., Jr.; Vreven, T.; Kudin, K. N.; Burant, J. C.; Millam, J. M.; Iyengar, S. S.; Tomasi, J.; Barone, V.; Mennucci, B.; Cossi, M.; Scalmani, G.; Rega, N.; Petersson, G. A.; Nakatsuji, H.; Hada, M.; Ehara, M.; Toyota, K.; Fukuda, R.; Hasegawa, J.; Ishida, M.; Nakajima, T.; Honda, Y.; Kitao, O.; Nakai, H.; Klene, M.; Li, X.; Knox, J. E.; Hratchian, H. P.; Cross, J. B.; Bakken, V.; Adamo, C.; Jaramillo, J.; Gomperts, R.; Stratmann, R. E.; Yazyev, O.; Austin, A. J.; Cammi, R.; Pomelli, C.; Ochterski, J. W.; Ayala, P. Y.; Morokuma, K.; Voth, G. A.; Salvador, P.; Dannenberg, J. J.; Zakrzewski, V. G.; Dapprich, S.; Daniels, A. D.; Strain, M. C.; Farkas, O.; Malick, D. K.; Rabuck, A. D.; Raghavachari, K.; Foresman, J. B.; Ortiz, J. V.; Cui, Q.; Baboul, A. G.; Clifford, S.; Cioslowski, J.; Stefanov, B. B.; Liu, G.; Liashenko, A.; Piskorz, P.; Komaromi, I.; Martin, R. L.; Fox, D. J.; Keith, T.; AlLaham, M. A.; Peng, C. Y.; Nanayakkara, A.; Challacombe, M.; Gill, P. M. W.; Johnson, B.; Chen, W.; Wong, M. W.; Gonzalez, C.; Pople, J. A. *Gaussian09, revision B.01*; Gaussian, Inc.: Pittsburgh, PA, 2004.
- Singh, U. C.; Kollman, P. A. *J. Comput. Chem.* **1984**, *5*, 129–145.
- Estiu, G.; Merz, K. M., Jr. *Biochemistry* **2006**, *45*, 4429–4443.
- Adam, K. R.; Antolovich, M.; Baldwin, D. S.; Brigden, L. G.; Duckworth, P. A.; Lindoy, L. F.; Bashall, A.; Mcpartlin, M.; Tasker, P. A. *J. Chem. Soc., Dalton Trans.* **1992**, *12*, 1869–1876.
- Hornak, V.; Abel, R.; Okur, A.; Strockbine, B.; Roitberg, A.; Simmerling, C. *Proteins: Struct. Funct. Bioinform.* **2006**, *65*, 712–725.

- (33) Jorgensen, W. L.; Chandrasekhar, J.; Madura, J. D.; Impey, R. W.; Klein, M. L. *J. Chem. Phys.* **1983**, *79*, 926–935.
- (34) Aqvist, J. *J. Phys. Chem.* **1990**, *94*, 8021–8024.
- (35) Smith, D.; Dang, L. *J. Chem. Phys.* **1994**, *100*, 3757–3766.
- (36) Berendsen, H. J. C.; Postma, J. P. M.; van Gunsteren, W. F.; DiNola, A.; Haak, J. R. *J. Chem. Phys.* **1984**, *81*, 3684–3690.
- (37) Phillips, J. C.; Braun, R.; Wang, W.; Gumbart, J.; Tajkhorshid, E.; Villa, E.; Chipot, C.; Skeel, R. D.; Kale, L.; Schulten, K. *J. Comput. Chem.* **2005**, *26*, 1781–1802.
- (38) Pettersen, E. F.; Goddard, T. D.; Huang, C. C.; Couch, G. S.; Greenblatt, D. M.; Meng, E. C.; Ferrin, T. E. *J. Comput. Chem.* **2004**, *25*, 1605–1612.
- (39) Garcia, A. E. *Phys. Rev. Lett.* **1992**, *68*, 2696–2699.
- (40) Aleksiev, T.; Potestio, R.; Pontiggia, F.; Cozzini, S.; Micheletti, C. *Bioinformatics* **2009**, *25*, 2743–2744.
- (41) Micheletti, C.; Carloni, P.; Maritan, A. *Proteins* **2004**, *55*, 635–645.
- (42) Pervushin, K.; Riek, R.; Wider, G.; Wuthrich, K. *Proc. Natl. Acad. Sci. U.S.A.* **1997**, *94*, 12366–12371.
- (43) Bertini, I.; Felli, I. C.; Kummerle, R.; Moskau, D.; Pierattelli, R. *J. Am. Chem. Soc.* **2004**, *126*, 464–465.
- (44) Silva, J. R. A.; Lameira, J.; Santana, P. P. B.; Silva, A.; Schneider, M. P. C.; Alves, C. N. *Int. J. Quantum Chem.* **2010**, *110*, 2067–2075.
- (45) Yarnitzky, T.; Levit, A.; Niv, M. Y. *Curr. Opin. Drug Discovery Dev.* **2010**, *13*, 317–325.
- (46) Yi, M.; Tjong, H.; Zhou, H. X. *Proc. Natl. Acad. Sci. U.S.A.* **2008**, *105*, 8280–8285.
- (47) Zhang, Y.; Sham, Y. Y.; Rajamani, R.; Gao, J.; Portoghese, P. S. *ChemBioChem* **2005**, *6*, 853–859.
- (48) Law, R. J.; Sansom, M. S. *Eur. Biophys. J.* **2004**, *33*, 477–489.
- (49) Capener, C. E.; Shrivastava, I. H.; Ranatunga, K. M.; Forrest, L. R.; Smith, G. R.; Sansom, M. S. *Biophys. J.* **2000**, *78*, 2929–2942.
- (50) Potestio, R.; Pontiggia, F.; Micheletti, C. *Biophys. J.* **2009**, *96*, 4993–5002.
- (51) Cascella, M.; Micheletti, C.; Rothlisberger, U.; Carloni, P. *J. Am. Chem. Soc.* **2005**, *127*, 3734–3742.
- (52) Carnevale, V.; Raugei, S.; Micheletti, C.; Carloni, P. *J. Am. Chem. Soc.* **2006**, *128*, 9766–9772.
- (53) Pontiggia, F.; Colombo, G.; Micheletti, C.; Orland, H. *Phys. Rev. Lett.* **2007**, *98*, 048102.
- (54) Boehr, D. D.; Nussinov, R.; Wright, P. E. *Nat. Chem. Biol.* **2009**, *5*, 789–796.

CT900635Z